Polarized microtubule arrays in apical dendrites and axons

Alex C. Kwan, Daniel A. Dombeck*, and Watt W. Webb†

School of Applied and Engineering Physics, Cornell University, Ithaca, NY 14853

Contributed by Watt W. Webb, May 29, 2008 (sent for review April 7, 2008)

The polarization of microtubules within neurons *in vivo* is crucial in their role of determining the directions and speeds of intracellular transport. More than a decade ago, electron microscopy studies of mature hippocampal cultures indicated that their axons contained microtubules of uniform polarity and that dendrites contained microtubules of mixed polarity. Here, we evaluated polarity distributions in native brain tissues and in cultures by using multiphoton microscopy and second-harmonic generation from microtubules. We confirmed the expected polarized microtubule arrays in axons; however, we also unexpectedly found them ubiquitously in apical dendrites of mature hippocampal CA1 and cortical layer V pyramidal neurons. Some of these organized dendritic microtubule arrays extended for >270 μm with overall polarity of >80%. Our research indicates neurite-specific and age-dependent microtubule organizations that have direct implications for neuronal cargo transport.

multiphoton microscopy | neurons | second-harmonic generation | intracellular transport

Active intracellular transport along microtubules is essential for establishing and maintaining the functions of axons and dendrites. Anterograde transport through neurites delivers cargoes that are produced in the soma, including postsynaptic densities, neurotransmitter receptors, ion channels, and specific mRNAs to dendritic locations, as well as components of presynaptic terminals, adhesion molecules, and mitochondria to axonal locations (1, 2). These cargoes are transported by molecular motors, such as kinesin and dynein, which tread unidirectionally on microtubules. To understand this directional trafficking (3–6), it is essential to know both the motor proteins and the microtubule polarities involved. Recently, great progress has been made in elucidating the numerous motor proteins, including the molecular and functional classification of their superfamilies (1, 7, 8), but few studies have characterized the microtubule organization in neurons, particularly in dendritic processes.

Past studies of microtubule polarity used electron microscopy to visualize neurites that were lysed in a tubulin-containing buffer, which would decorate clockwise or counterclockwise "hooks" on microtubules depending on their polarity (9). The hook method, applied on hippocampal cultures (10–12), indicated that microtubule arrays have uniform polarity (≈100% plus-ends distal from soma) in neurites of nascent neurons, uniform polarity in mature axons, and mixed polarity (≈50% plus-ends and ≈50% minus-ends distal from soma) in mature proximal dendrites. This difference between axons and dendrites of cultured hippocampal neurons had been implicated as a milestone in the establishment of neuronal polarity (13). However, the requirement of thin, fixed sections for electron microscopy (10, 11) has limited successful application of the hook method to only a few tissue preparations (14, 15). Recently, fluorescently labeled plus-end tracking proteins have been used to estimate microtubule polarity in fruit flies (16) but not yet in mammals.

Second-harmonic generation (SHG) microscopy can image noncentrosymmetric protein structures with high hyperpolarizability, such as collagen and microtubules (17–19), but few other known protein structures. SHG, as a nonlinear optical process, occurs in microtubules because tubulin is hyperpolarizable and asymmetric along its longitudinal axis; therefore, adjacent microtubules of the same polarity constitute an array of aligned scattering dipoles that, through constructive interference (20), emit a coherent optical signal at exactly half the excitation wavelength. Conversely, emitted fields from adjacent microtubules of opposite polarities would destructively interfere and eliminate or degrade the SHG signal. Thus, the SHG signal comes from microtubule arrays that have parallel polarization. However, SHG intensity alone does not distinguish the sign of net orientation between plus- or minus-end-oriented arrays. SHG has been used as an imaging tool in living preparations (21–27) to identify polarized microtubule arrays in mitotic spindles of RBL cells (17) and *Caenorhabditis elegans* embryos (18, 19) and in cilia (17). Polarized microtubule arrays were also found in hippocampal slices in our earlier research (17), where we looked at tissues from young rat pups. Here, we extend the research to brain slices of mice of older age groups and show that the microtubule polarity in dendrites is age-dependent, with significant differences between neurons in cultures and in mature brain tissues.

Results

Polarized Microtubule Arrays Are Localized to Apical Dendrites and to Axons in Adult Mice. To investigate regional differences of microtubule polarity, we imaged acute brain slices with SHG microscopy. In the hippocampus of a 5-month-old mouse, we found the expected SHG in the axonal mossy fiber, which we had seen in younger animals (17), but surprisingly the CA1 stratum radiatum also generated SHG (Fig. 1*A*), which was not seen before. This finding was unexpected because stratum radiatum is known to be predominantly dendritic (28).

To identify more accurately the types of neurites that contain polarized microtubule arrays, we used multiphoton microscopy (29, 30) and SHG microscopy to image acute slices of 4- to 12-month-old transgenic mice that express YFP controlled by *Thy1*-promoter (*Thy1*-YFP line-H) (31). This strain labels neurons exclusively, enabling us to compare SHG with neuronal morphology. The SHG was seen to localize to proximal apical dendrites of CA1 pyramidal neurons (Fig. 1 *B* and *C*). In adult mice (n = 5; >4 months old), we found that 41 of 45 (91%) YFP-labeled pyramidal neurons emitted SHG. Because not all neurons expressed YFP, we also observed SHG from apical

Author contributions: A.C.K., D.A.D., and W.W.W. designed research; A.C.K. performed research; A.C.K. analyzed data; and A.C.K. and W.W.W. wrote the paper.

The authors declare no conflict of interest.

Freely available online through the PNAS open access option.

*Present address: Molecular Biology Department and Princeton Neuroscience Institute, Princeton University, Princeton, NJ 08544.

†To whom correspondence should be addressed at: School of Applied and Engineering Physics, Cornell University, 223 Clark Hall, Cornell University, Ithaca, NY 14853. E-mail: www2@cornell.edu.

This article contains supporting information online at www.pnas.org/cgi/content/full/0805199105/DCSupplemental.

© 2008 by The National Academy of Sciences of the USA

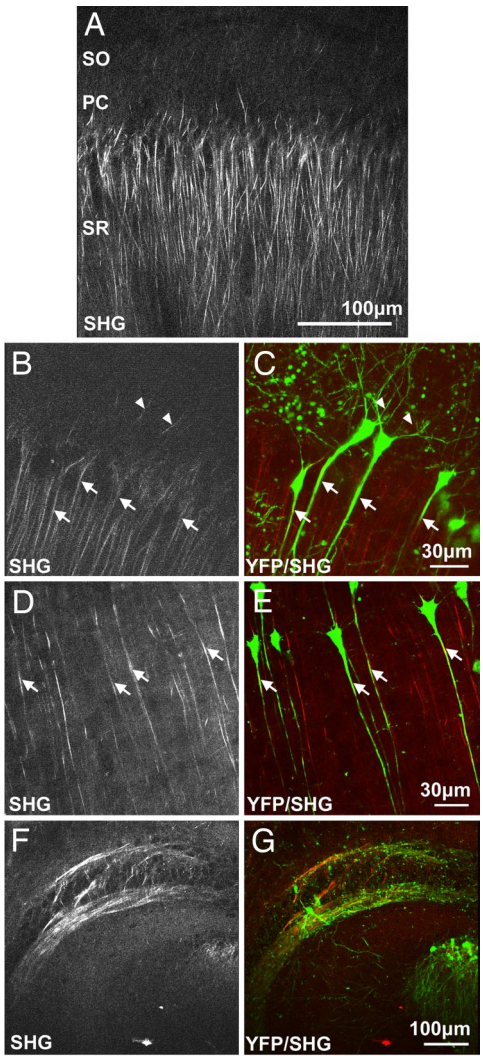

Fig. 1. Polarized microtubule arrays in acute brain slices of adult wild-type and *Thy1*-YFP mice. (*A*) SHG in area CA1 of an acute hippocampal slice of a 5-month-old wild-type mouse. Subregions stratum oriens (SO), pyramidal cells (PC), and stratum radiatum (SR) can be identified by autofluorescence (data not shown). (*B*) SHG in area CA1 of a 5-month-old *Thy1*-YFP mouse. (*C*) Composite image of multiphoton-excited YFP fluorescence (green) and SHG (red) at the same location as *B*. Polarized microtubule arrays colocalize with apical dendrites of CA1 pyramidal neurons (arrows). SHG also appears in stratum oriens and is likely caused by axons (solid triangles). (*D* and *E*) SHG and composite image in neocortex of an acute coronal cortical slice of an 11-month-old *Thy1*-YFP mouse. Polarized microtubule arrays colocalize with apical dendrites of layer V pyramidal neurons (arrows). (*F* and *G*) SHG and composite image in area CA3 of a 5-month-old *Thy1*-YFP mouse. Polarized microtubule arrays colocalize with the dense axonal bundle that forms the mossy fiber. All images are projections of three to six optical z-sections taken 10 μm apart with laser excitation at 774 nm that has linear polarization oriented along the apical dendrites.

dendrites of unlabeled pyramidal neurons. The number of all SHG-emitting dendrites is comparable with the expected number of CA1 neurons in adult mice (32). These data suggest that virtually all apical dendrites contain polarized microtubule arrays. We also observed SHG in the region stratum oriens. Because these signals were sparse, we reasoned that they did not originate from basal dendrites, which are ubiquitous in the region, but instead came from CA1 axons that could project laminarly for a short distance before descending to the subiculum (28). Because there are no immature neurons in area CA1 of the

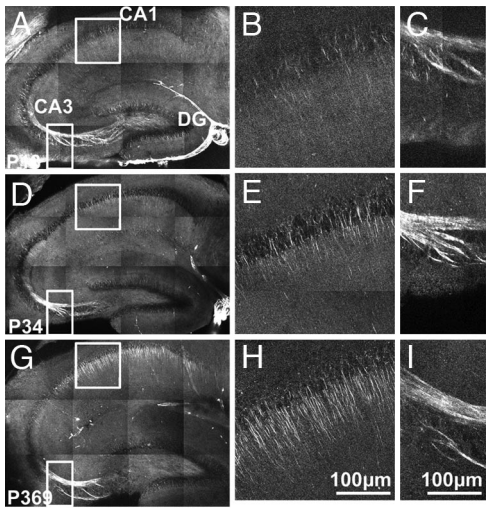

Fig. 2. Polarized microtubule arrays in acute hippocampal slices of young, juvenile, and adult mice. (*A*) SHG in hippocampus of a postnatal day 13 (P13) mouse. The patchy background is caused by weak autofluorescence that is picked up by the SHG detector. (*B* and *C*) Magnified SHG views of the area CA1 and the mossy fiber from the boxed areas in *A*. (*D–F*) Same as *A–C* of a P34 mouse. (*G–I*) Same as *A–C* of a P369 mouse. Images are mosaics of 12 projections of optical z-sections at 15 μm apart with laser excitation at 774 nm that has linear polarization oriented along the apical dendrites.

adult hippocampus (33), we conclude that the SHG there comes from apical dendrites of mature CA1 pyramidal neurons. In the neocortex (Fig. 1 *D* and *E*), we found colocalization of YFP fluorescence and SHG in 36 of 41 (88%) layer V pyramidal neurons in adult mice ($n = 2$). Polarized microtubule arrays in apical dendrites extended to 270 μm, with an average distance of 201 $\pm$ 37 μm, toward upper cortical layers. In contrast, basal and oblique dendrites did not generate detectable SHG. In area CA3 (Fig. 1 *F* and *G*), SHG was emitted from the mossy fiber, an unmyelinated axonal bundle. Our data in the hippocampus and in the neocortex of adult mice suggest that polarized microtubule arrays exist not only in axons, but also in large stretches of apical dendrites of pyramidal neurons.

Distribution of Polarized Microtubule Arrays Depends on Age. To determine whether the distribution of polarized microtubule arrays in native brain tissue depends on development, we imaged hippocampi of mice 1 week to >18 months old (Fig. 2; $n = 27$ mice) and found consistent trends among mice of same age groups. For axons, the mossy fiber contained polarized microtubule arrays in young mice and maintained polarity into late adulthood. Additional SHG signals were often seen in neurites lining the CA3 and dentate gyrus cell layers that funnel into the mossy fiber in mice <1 month old. For CA1 apical dendrites, polarized microtubule arrays existed but were relatively sparse and short in young mice (Fig. 2*B*). At 1 month old, arrays became discernable and increased in both density and length, initially in the CA1 pyramidal cell layer and subsequently in the stratum radiatum (Fig. 2*E*). These polarized microtubule arrays grew to $\approx$90 μm long until the mice were 4 months old and then did not change significantly (Fig. 2*H*). The observed changes could be caused by either a polarity change in the existing microtubule array or the addition of new polarized microtubules. Polarized microtubule arrays in area CA1 were seen in ages up to the oldest mice investigated (18 months old). The developmental change in the structure of these microtubule arrays is quantified by data plots in Fig. 3. Our data show that polarized microtubule distribution in neuronal processes is dynamic within a period of rapid learning and development in the lifetime of the mouse.

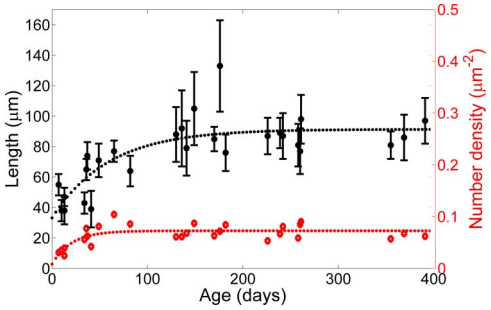

Fig. 3. Age dependence of length and number density of polarized microtubule arrays in area CA1. The length of polarized microtubule arrays is the extent to which SHG-emitting neurites extend from the pyramidal cell layer in area CA1. Each point is an average of 10 neurites, and the error bars are ±SD. An exponential fit illustrates the trend. The number density counts the number of SHG-emitting neurites within an image and divides that number by the length of the CA1 cell layer and the depth of an optical section, which is ≈2 μm. In adult mice, our measured density of 0.07 μm^{-2} would yield ≈2 $\times 10^5$ CA1 pyramidal neurons in one hippocampus that is 1.5 mm thick with a 2-mm-long CA1 cell layer.

Numerical Simulation of SHG from a Microtubule Array. To estimate quantitatively the microtubule polarity, numerical simulations calculated the amount of SHG generated from a microtubule array. The physics of SHG is well understood, and studies (20, 23) have derived the theory for excitation by a focused laser beam (see supporting information (SI) *Methods*).

The absolute SHG intensity depends on the laser power and the hyperpolarizability, number density, spacing, and polarity of the microtubules. Microtubule number density and spacing can be estimated because we have two pieces of *a priori* knowledge about the spatial arrangement of the dipoles: (*i*) The dipoles, presumably tubulins, line up in helical arrays to form a microtubule; (*ii*) The mean distance between microtubules in neurites is set by microtubule-associated proteins (MAPs), as has been measured by electron microscopy (34). Furthermore, we assumed the extent of the tubule array to be approximately the size of a typical neurite (35). With these parameters, we calculated forward- and backward-directed intensities of SHG caused by single neurites (Fig. 4*A* and Fig. S2) for increasing microtubule polarity. It is illuminating to compare the simulated forward-directed SHG intensities (Fig. 4*B*, circles) with simple quadratic equations (Fig. 4*B*, solid lines) that consider interference and SHG as a second-order process. The fits are best near uniform polarity and deviate slightly at mixed polarity because the microtubules are spatially distributed and therefore their SHG fields do not exactly cancel destructively. This quadratic dependence makes signal intensity a good qualitative indicator of microtubule polarity because a small decline in polarity would cause a large drop in intensity.

Further examination of the theory (see *SI Methods*) shows that laser power and hyperpolarizability scale linearly with forward- and backward-directed SHG intensities; thus, they do not affect the ratio of forward- over backward-directed SHG intensity (f/b SHG ratio). Therefore, given assumptions about the microtubule number density and spacing, the f/b SHG ratio can be directly related to microtubule polarity (Fig. 4*C*). In practice, the f/b SHG ratio is also easier to measure than absolute SHG intensity because it is difficult to determine sample hyperpolarizability.

Measuring the Polarity of Microtubule Arrays Within Neurites. To verify the validity of our approach of using the f/b SHG ratio to estimate microtubule polarity, we made measurements in hippocampal cultures, where published values of polarity exist based on the hook method. Immature and mature neurons were identified separately by staining for Tau-1 and MAP-2. After 2–3 days in culture, developing neurons possessed multiple minor processes and sometimes had nascent axons, which all contained polarized microtubule arrays (Fig. 5 *A–C*). In cultures >7 days old, we distinguished axons and dendrites of mature neurons by using MAP-2 as a specific marker for dendrites (36). Polarized microtubule arrays were found in axons (Fig. 5 *E–H*) but were absent in the dendrites that could be clearly distinguished. Measurements from Tau-1-stained axons produced an f/b SHG ratio of 20 ± 2, which translates to a microtubule polarity of ≈100% (+0%, −22%) (see *SI Methods* for error analysis). In comparison, past studies with the hook method found polarities of 57 ± 4% for dendrites and 99 ± 4% for axons in mature neurons. Our observations of developmental changes agree with past observations (10, 11) that, in cultures, protoprocesses of immature neurons and axons of mature neurons have uniform polarity microtubules, whereas dendrites have mixed polarity microtubules.

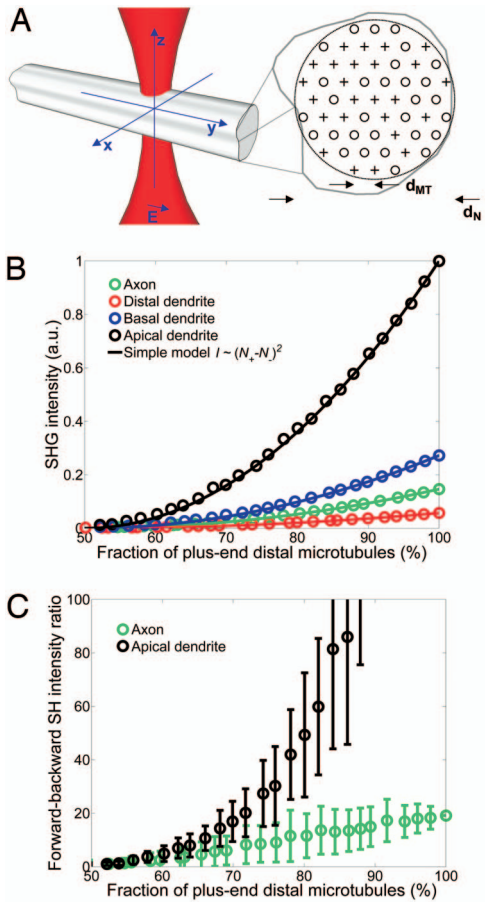

Fig. 4. Numerical simulation of SHG generated by a microtubule array. (*A*) Schematic drawing of the simulation model. A focused laser beam impinges on a neurite with diameter d_N that contains a hexagonal packed array of plus- or minus-end distal microtubules with intermicrotubule spacing d_{MT}. SHG intensities were calculated in the forward and backward directions for four classes of neurites: apical dendrites (d_{MT} = 64 nm, d_N = 3 μm), basal dendrites (d_{MT} = 64 nm, d_N = 1 μm), distal dendrites (d_{MT} = 64 nm, d_N = 0.5 μm), and axons (d_{MT} = 22 nm, d_N = 0.17 μm). (*B*) Simulated forward-directed SHG intensities generated by each type of neurite (circles). Polarity is defined as the number of plus-end distal microtubules divided by the total number of microtubules in the simulated neurite. The simulated intensities were compared with a simple model (solid line) where SHG intensity $\sim [N_+ - N_-]^2$, where N_+ and N_- are the numbers of plus- and minus-end distal microtubules. Backward-directed signals are too small to be shown in the same vertical scale. (*C*) Simulated fb SHG intensity ratio. The error bars are ±SD. Uncertainty is caused by the possible variety of microtubule distributions that can be arranged within a neurite.

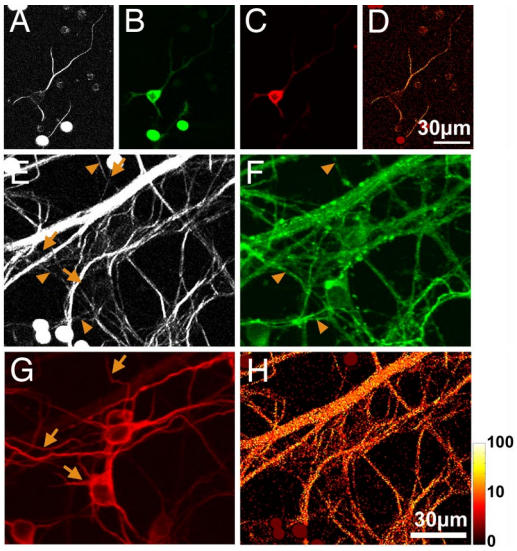

Fig. 5. Measuring microtubule polarity in dissociated hippocampal cultures. (*A*) SHG from neurons 3 days in culture. Protoprocesses in neurons at this stage contain polarized microtubule arrays. The solid circles with saturated fluorescence signal are beads added to calibrate the SHG detectors. (*B* and *C*) The same neuron fixed and stained for Tau-1 (green) and MAP-2 (red), which were localized to the soma in immature neurons. (*D*) Pixel-by-pixel forward–backward intensity ratios calculated from *A*. (*E–H*) Same as *A–D* but from neurons 9 days in culture. SHG and Tau-1 were present in the axons (solid triangles), but SHG was absent in the dendrites, which contains MAP-2 (arrows). The SHG images were taken with circularly polarized excitation at 854 nm.

Using the same methods, we quantified microtubule polarity in acute brain slices that were flattened to 30–50 μm thick to minimize backscattered signal. From axons in the hippocampal mossy fiber of adult mice, we measured an f/b SHG ratio of 27 ± 5, which corresponds to mean microtubule polarity of ≈100% (+0%, −17%). The f/b SHG ratio of axons in acute slices was higher than expected from the simulation, a difference that could be caused by a higher packing density of microtubules in axons in acute slices. From apical dendrites, in the area CA1 of adult mice (Fig. 6) we found mean polarity of 81% (+7%, −9%), and in the layer V cortex, mean polarity of 80% (+6%, −6%), which correspond to f/b SHG ratios of 53 ± 27 and 50 ± 12, respectively.

Importantly, the f/b SHG ratio is not strictly a result of strong SHG; it depends on the spatial distribution of the scatterers. This is shown by SHG from the collagen matrix surrounding blood vessels (Fig. 6), which exhibit a modest f/b SHG ratio of ≈4 (23). Although basal dendrites did not produce detectable SHG, we found by comparing the intensities recorded from the neuropil in the apical and basal sides of the CA1 cell layer that our detection sensitivity places an upper limit of ≈65% on the microtubule polarity in basal dendrites, indicating that the basal dendrites could contain microtubules with <65% overall polarity.

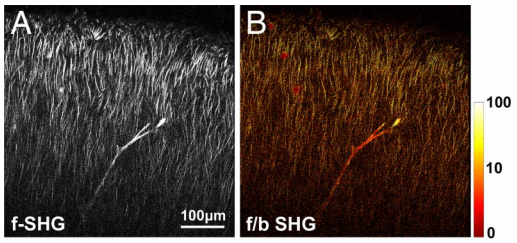

Fig. 6. Measuring microtubule polarity in acute brain slices. (*A*) Measured forward-directed SHG (f-SHG) images in area CA1 of an 8-month-old wild-type mouse. A Y-shaped blood vessel is visible. (*B*) Pixel-by-pixel f/b SHG ratios calculated from *A*. Image was taken with laser excitation at 854 nm that has linear polarization oriented along the apical dendrites.

Discussion

Comparison of Methods for Measuring Microtubule Polarity. There is strong evidence that the optical signal in SHG imaging of brain tissues reported here originates from polarized microtubules. SHG is rare in biology, occurring only in asymmetric, optically nonlinear structures, hyperpolarizable with large-scale order; therefore, only a few biological systems (e.g., collagen, membrane labeled with noncentrosymmetric dyes) are known to emit SHG. The microtubule origin of SHG is effectively shown in intact brain slices by noticeable loss of signal after application of the microtubule-depolymerizing drug nocodazole (ref. 17; see also Fig. S1). Moreover, SHG from MAPs seems unlikely because SHG is seen in many microtubule-containing structures—axons, cilia, and mitotic spindles—with differing MAP compositions (17, 19). Finally, the requirement of same polarity is supported by the inherent physical requirement for constructive interference, the lack of SHG signal in the overlapping zones in mitotic spindle (17, 19), and the axon–dendrite difference in hippocampal cultures.

Currently, there are two other techniques for establishing microtubule polarity, the hook method and fluorescently labeled plus-end tracking proteins. The hook method uses electron microscopy, which provides sufficient resolution for counting individual microtubules. It requires fixation and is quantitatively uncertain because of a large "unhooked" fraction from unstained microtubules. Using fluorescently labeled plus-end tracking proteins requires transgenic specimens or cells accessible to transfection because fluorescent proteins must be introduced. Quantification is indirect because it assumes that the trafficking patterns of plus-end tracking proteins reflect the polarity of the whole microtubule array, thus risking biased preference for actively polymerizing microtubules.

Because SHG microscopy requires no external perturbation, it can determine microtubule polarity in native tissues where fixation or transfection is prohibitive. However, the method has two limitations: quantification and determination of the sign of polarity. As shown here, polarity can be quantified by f/b SHG ratio measurements. Our culture experiments confirmed the simulation results with positive (uniform polarity in axons) and negative (mixed polarity in dendrites) tests. Further tests at intermediate polarity values would require artificial assemblies of microtubule bundles with specific spacing and polarity. The SHG quantification of polarity requires knowledge of the spatial arrangement of microtubules, which must be estimated with electron microscopy (35) or superresolution immunohistochemistry (37). Measuring the weak backward-directed SHG and estimating structural quantities can be subject to rather large uncertainties. Such structural parameters as dendrite thickness and microtubule packing density can influence SHG intensity, although the main determinant is polarity. For example, SHG intensity would drop by ≈70% if the polarity changed from 100% to 75% in a 3-μm-diameter neurite, but the same intensity drop would require a 9-fold shrinkage in cross-sectional area (Fig. 4*B*, solid lines). Determining the absolute sign of the microtubule polarity requires determination of the phase of emitted SHG relative to a reference sample or complementary information from transport studies.

Implications for Dendritic Transport. Our research reveals that polarized microtubule arrays are found both in axons and in a substantial subset of mature dendrites in native brain tissue (Table 1). Although axons generally contain polarized microtubule arrays throughout development, the microtubule distribu-

NEUROSCIENCE

Table 1. Microtubule polarity distribution within identified neurite groups in brain tissue and hippocampal culture

Neurite type	Region in the brain	Measured f/b SHG ratio	Microtubule polarity, % (uncertainties, %)
Axons	Mossy fiber (dentate gyrus to CA3)	27 ± 5	100 (+0, −17)
Axons	Hippocampal culture	20 ± 2	100 (+0, −22)
Apical dendrites	CA1	53 ± 27	81 (+7, −9)
Apical dendrites	Layer V neocortex	50 ± 12	80 (+6, −6)
Basal dendrites	CA1	NA	<65

tion in apical dendrites is age-dependent, showing mixed polarity at early ages and increasing overall polarity up to 4 months of age. These results contrast with the usual interpretation of the known information on microtubule polarity inferred from cultured neurons where only axons and the distal dendritic tips contained polarized microtubule arrays in mature neurons. Furthermore, our result is consistent with previous research (17) using young rat pups where SHG was observed in axons. Therefore, our research indicates a critical revision of the canonical model of microtubule organization in specific fractions of dendrites *in vivo*.

The concept that apical dendrites contain polarized microtubule arrays suggests that either plus-end- or minus-end-directed motor proteins, but not both types, are responsible for anterograde movement during transport, because plus-end- and minus-end-directed motor proteins would move in opposite directions. SHG imaging alone does not provide the sign of the polarity of the microtubule arrays; studies have shown that kinesin is responsible for anterograde cargo movement in dendrites, (*cf.* ref. 1), which indicates that microtubules in proximal apical dendrites are uniformly plus-end distal from the soma.

On average, proximal apical dendrites of CA1 and cortical layer V pyramidal neurons extend for ≈100 μm and ≈200 μm, respectively, before bifurcating, the same lengths found to contain polarized microtubule arrays. The benefit of such a uniaxial array is speed: primarily unidirectional transport of anterograde cargoes is thought to be more efficient. A biophysical model of active transport (38) has predicted that the anterograde flux in unidirectional transport is ≈10 times faster than in bidirectional transport for a 100-μm-long neurite because in unidirectional transport, cargoes spend more time actively moving toward the destination. *In vivo*, cargo delivery is slowed further by MAPs that obstruct and reduce motor protein processivity (39). An order of magnitude difference in transit time can be critical for time-limited processes, such as activity-dependent transport of newly expressed mRNAs from the soma (40, 41), where local protein synthesis can participate in long-term synaptic plasticity, but only in a narrow time window during or shortly after induction (42). Therefore, modification of microtubule organization, for example, caused by aging as our work shows, could be regulating these time-limited processes.

A series of trafficking experiments in conjunction with measurements of microtubule polarity could further elucidate the transport mechanisms within dendritic subtypes. Our observation that dendrites can have differential microtubule organization can be useful for interpreting time-lapse trafficking studies, where past reports found differential RNA transport velocities for long versus short dendrites (4), primarily anterograde kinesin-based transport in apical dendrites (5), and primarily distal end-directed displacements of plus-end tracking proteins (6). Application of our results to research on the neuronal microtubule network should help to contextualize the flourishing number of motor protein and trafficking studies.

Materials and Methods

Acute Brain Slices. All preparations were performed in accordance with Cornell University animal use regulations (IACUC protocol 00-46-03). Wild-type C57BL/6 (Charles River) or transgenic mice that express YFP under the Thy1 promoter [strain B6.Cg-Tg(*Thy1*-YFPH)2Jrs/J); Jackson Laboratories] were purchased and housed in the Laboratory Animal Services. The brain was removed after CO_2 euthanasia of mice older than postnatal day 10 and decapitation of pups. Transverse hippocampal or coronal cortical slices 400 μm thick were cut in a Vibratome (Campden Instruments) at ≈4°C in artificial cerebrospinal fluid (ACSF) composed of 120 mM NaCl, 2.5 mM KCl, 1 mM NaH_2PO_4, 1.3 mM $MgSO_4$, 25 mM $NaHCO_3$, 10 mM D-glucose, and 2.5 mM $CaCl_2$ and was saturated with 95% O_2 and 5% CO_2. Dissection and cutting were performed quickly to minimize damage. Slices were then incubated in ACSF at 35°C for 1 h before imaging. During imaging, slices were held under nylon grid anchors in a flow chamber (Warner Instruments) continuously perfused with oxygenated ACSF at room temperature.

Primary Cultures. Hippocampal cultures were prepared as described in ref. 17. For immunohistochemistry, cultured neurons were fixed in 3.7% paraformaldehyde in PBS containing 15% sucrose at 4°C. Neurons were stained overnight with primary antibodies for Tau-1 (mouse, dilution 1:400; Chemicon) and MAP-2 (rabbit, 1:500; Chemicon) and then with secondary antibodies (Alexa Fluor 488 anti-mouse and Alexa Fluor 568 anti-rabbit, both from Invitrogen, 1:40). The samples were mounted in Vectashield antifade solution (Vector Laboratories) and imaged with a Bio-Rad MRC1024 confocal microscope equipped with an argon–krypton laser for excitation at 488 and 568 nm.

Imaging. For multiphoton and SHG imaging, we used a Bio-Rad MRC1024 scan head mounted on an inverted Olympus IX-70 microscope. Excitation was provided by a mode-locked Ti–sapphire laser (Spectra-Physics Tsunami). Beam intensity was controlled with a Pockels cell with flyback synchronization, and polarization was modified with a Berek compensator (New Focus). The excitation was focused with an Olympus UApo/340 20X/NA 0.7 water-immersion objective, and the forward emission was collected with an Olympus XLUMPlanFI 20X/NA 0.95 dipping objective. The average excitation laser intensity was 10–100 MW. SHG and fluorescence were collected in the forward and backward directions by bialkali photomultiplier tubes (Hamamatsu HC125-02) after infrared blocking filters (Semrock or Chroma Technology) and narrow bandpass filters with bandwidth of 10 nm (Semrock). Unless specified, images were obtained with SHG collected in the forward direction. SHG was verified by tuning the excitation wavelengths and observing the emission shift using narrowband filters. Because SHG intensity was weak, signal-to-noise was improved by averaging three to five scans that exposed the tissue for ≈6–10 s or by lowering the illumination intensity and then collecting in photon counting mode for 30–60 s. Quantitative image analysis was done with MATLAB and Alice (Perceptive Informatics).

SHG Intensity Ratio Measurements. Several drops of PBS mixed with 6-μm-diameter fluorescent beads (Fluoresbrite YG; Polyscience) were added to the culture dish by transfer pipette. Microtubules were imaged at a depth ≈10 μm below the beads. We measured the forward- and backward-directed SHG by photon counting at each pixel. To correct for background, we subtracted autofluorescence measured from adjacent empty regions. System detection efficiency was calibrated by measuring fluorescence of the beads. For acute slices, fluorescent beads were added to a transverse hippocampal or coronal slice 250 μm thick before the slice was placed between two glass coverslips so that, as in making wet-mount microscope slides, surface tension-induced adhesive forces would naturally draw the cover glasses together to yield a final interglass thickness of 30–50 μm. Thin slices were critical for reducing backscattered SHG (24, 27). Flattening might cause tissue damage, but a favorable comparison between normal tissues (Fig. 1*A*) and flattened tissues (Fig. 6*A*) showed that the effect on

microtubules is tolerable within the <10 min of time of individual imaging experiments. After flattening tissues, the SHG signal tends to endure for ≈30 min, whereas in normal tissue, SHG can be seen in acute slices for >4 h.

Numerical Simulation. Numerical simulation of SHG in the regime of focused laser beam that has been described (20, 23) is applied to microtubules in this research (see *SI Methods* for details).

ACKNOWLEDGMENTS. We thank M. Williams for editorial assistance, W. Zipfel and R. Williams for instrumentation help, and P. Gordnier and S. Kim for advice on growing cultures. This work was supported by National Institutes of Health Grant 9-P41-EB001976 (to W.W.W. and D.A.D.), National Institutes of Health Training Grant GM08267 (to D.A.D.), and by the Nanobiotechnology Center, a Science and Technology Center Program of the National Science Foundation under Agreement ECS-9876771 (to A.C.K.).

1. Hirokawa N, Takemura R (2005) Molecular motors and mechanisms of directional transport in neurons. *Nat Rev Neurosci* 6:201–214.
2. Hirokawa N (1998) Kinesin and dynein superfamily proteins and the mechanism of organelle transport. *Science* 279:518–526.
3. Vale RD, *et al.* (1996) Direct observation of single kinesin molecules moving along microtubules. *Nature* 380:451–453.
4. Davis L, Burger B, Banker GA, Steward O (1990) Dendritic transport: Quantitative analysis of the time course of somatodendritic transport of recently synthesized RNA. *J Neurosci* 10:3056–3068.
5. Guillaud L, Setou M, Hirokawa N (2003) KIF17 dynamics and regulation of NR2B trafficking in hippocampal neurons. *J Neurosci* 23:131–140.
6. Stepanova T, *et al.* (2003) Visualization of microtubule growth in cultured neurons via the use of EB3-GFP (end-binding protein 3-green fluorescent protein). *J Neurosci* 23:2655–2664.
7. Vale RD (2003) The molecular motor toolbox for intracellular transport. *Cell* 112:467–480.
8. Kanai Y, Dohmae N, Hirokawa N (2004) Kinesin transports RNA: Isolation and characterization of an RNA-transporting granule. *Neuron* 43:513–525.
9. Heidemann SR, McIntosh JR (1980) Visualization of the structural polarity of microtubules. *Nature* 286:517–519.
10. Baas PW, Black MM, Banker GA (1989) Changes in microtubule polarity orientation during the development of hippocampal neurons in culture. *J Cell Biol* 109:3085–3094.
11. Baas PW, Deitch JS, Black MM, Banker GA (1988) Polarity orientation of microtubules in hippocampal neurons: Uniformity in the axon and nonuniformity in the dendrite. *Proc Natl Acad Sci USA* 85:8335–8339.
12. Takahashi D, *et al.* (2007) Rearrangement of microtubule polarity orientation during conversion of dendrites to axons in cultured pyramidal neurons. *Cell Motil Cytoskel* 64:347–359.
13. Baas PW (1999) Microtubules and neuronal polarity: Lessons from mitosis. *Neuron* 22:23–31.
14. Burton PR (1988) Dendrites of mitral cell neurons contain microtubules of opposite polarity. *Brain Res* 473:107–115.
15. Rakic P, Knyihar-Csillik E, Csillik B (1996) Polarity of microtubule assemblies during neuronal cell migration. *Proc Natl Acad Sci USA* 93:9218–9222.
16. Rolls MM, *et al.* (2007) Polarity and intracellular compartmentalization of *Drosophila* neurons. *Neural Dev* 2:7.
17. Dombeck DA, *et al.* (2003) Uniform polarity microtubule assemblies imaged in native brain tissue by second-harmonic generation microscopy. *Proc Natl Acad Sci USA* 100:7081–7086.
18. Campagnola PJ, Loew LM (2003) Second-harmonic imaging microscopy for visualizing biomolecular arrays in cells, tissues and organisms. *Nat Biotechnol* 21:1356–1360.
19. Campagnola PJ, *et al.* (2002) Three-dimensional high-resolution second-harmonic generation imaging of endogenous structural proteins in biological tissues. *Biophys J* 82:493–508.
20. Moreaux L, Sandre O, Mertz J (2000) Membrane imaging by second-harmonic generation microscopy. *J Opt Soc Am B* 17:1685–1694.
21. Dombeck DA, Blanchard-Desce M, Webb WW (2004) Optical recording of action potentials with second-harmonic generation microscopy. *J Neurosci* 24:999–1003.
22. Dombeck DA, Sacconi L, Blanchard-Desce M, Webb WW (2005) Optical recording of fast neuronal membrane potential transients in acute mammalian brain slices by second-harmonic generation microscopy. *J Neurophysiol* 94:3628–3636.
23. Williams RM, Zipfel WR, Webb WW (2005) Interpreting second-harmonic generation images of collagen I fibrils. *Biophys J* 88:1377–1386.
24. Zipfel WR, *et al.* (2003) Live tissue intrinsic emission microscopy using multiphoton-excited native fluorescence and second- harmonic generation. *Proc Natl Acad Sci USA* 100:7075–7080.
25. Brown E, *et al.* (2003) Dynamic imaging of collagen and its modulation in tumors *in vivo* using second-harmonic generation. *Nat Med* 9:796–800.
26. Sacconi L, Dombeck DA, Webb WW (2006) Overcoming photodamage in second-harmonic generation microscopy: Real-time optical recording of neuronal action potentials. *Proc Natl Acad Sci USA* 103:3124–3129.
27. Debarre D, *et al.* (2006) Imaging lipid bodies in cells and tissues using third-harmonic generation microscopy. *Nat Methods* 3:47–53.
28. Johnston D, Amaral DG (2004) in *The Synaptic Organization of the Brain*, ed Shepherd GM (Oxford Univ Press, New York), pp 455–498.
29. Denk W, Strickler JH, Webb WW (1990) Two-photon laser scanning fluorescence microscopy. *Science* 248:73–76.
30. Zipfel WR, Williams RM, Webb WW (2003) Nonlinear magic: Multiphoton microscopy in the biosciences. *Nat Biotechnol* 21:1369–1377.
31. Feng G, *et al.* (2000) Imaging neuronal subsets in transgenic mice expressing multiple spectral variants of GFP. *Neuron* 28:41–51.
32. Calhoun ME, *et al.* (1998) Hippocampal neuron and synaptophysin-positive bouton number in aging C57BL/6 mice. *Neurobiol Aging* 19:599–606.
33. Lledo PM, Alonso M, Grubb MS (2006) Adult neurogenesis and functional plasticity in neuronal circuits. *Nat Rev Neurosci* 7:179–193.
34. Chen J, Kanai Y, Cowan NJ, Hirokawa N (1992) Projection domains of MAP-2 and tau determine spacings between microtubules in dendrites and axons. *Nature* 360:674–677.
35. Fiala JC, Harris KM (1999) *Dendrites*, eds Stuart G, Spruston N, Hausser M (Oxford Univ Press, New York), pp 1–34.
36. Ferreira A, Busciglio J, Cáceres A (1987) An immunocytochemical analysis of the ontogeny of the microtubule-associated proteins MAP-2 and Tau in the nervous system of the rat. *Brain Res* 431:9–31.
37. Bates M, Huang B, Dempsey GT, Zhuang X (2007) Multicolor superresolution imaging with photo-switchable fluorescent probes. *Science* 317:1749–1753.
38. Smith DA, Simmons RM (2001) Models of motor-assisted transport of intracellular particles. *Biophys J* 80:45–68.
39. Seitz A, *et al.* (2002) Single-molecule investigation of the interference between kinesin, tau and MAP-2c. *EMBO J* 21:4896–4905.
40. Steward O, Worley PF (2001) Selective targeting of newly synthesized Arc mRNA to active synapses requires NMDA receptor activation. *Neuron* 30:227–240.
41. Grooms SY, *et al.* (2006) Activity bidirectionally regulates AMPA receptor mRNA abundance in dendrites of hippocampal neurons. *J Neurosci* 26:8339–8351.
42. Sutton MA, Schuman EM (2006) Dendritic protein synthesis, synaptic plasticity, and memory. *Cell* 127:49–58.